Experimental spectra, electronic properties (liquid and gaseous phases) and activity against SARS-CoV-2 main protease of Fluphenazine dihydrochloride: DFT and MD simulations

Jamelah S. Al-Otaibi [a,*], Y. Sheena Mary [b,c], Y. Shyma Mary [b], R. Niranjana Devi [d], Sreejit Soman [e]

[a] *Department of Chemistry, College of Science, Princess Nourah Bint Abdulrahman University, P.O. Box 84428, Riyadh 11671, Saudi Arabia*
[b] *Thushara, Neethinagar-64, Pattathanam, Kollam, Kerala, India*
[c] *Department of Physics, FMNC, Kollam, Kerala, India*
[d] *Department of Physics, Fatima College, Madurai, Tamilnadu, India*
[e] *Stemskills Research and Education Lab Private Limited, Faridabad, Hariyana, India*

ABSTRACT

The Gaussian 09 DFT tool is used to investigate the formational electronic behaviour, reactivity analysis and biological properties of fluphenazine dihydrochloride (FDD). The quantum computation is used to determine the spectroscopic and vibrational assignments of FDD. The NBO method explains charge transfer and molecular interactions. Energy gap values are determined using FMO analysis in different solvents and toluene is a better solvent due to higher value of solvation energy. The UV-visible spectra are investigated in various solvents using the TD-DFT method. Electrostatic potential, the wave function related properties such as LOL, NCI and RDG are determined in gaseous phase. Furthermore, the drug likeness is analyzed. At last, a docking study with MD simulation is used to investigate FDD's antiviral activity against SARS-CoV-2 main protease.

© 2022 Elsevier B.V. All rights reserved.

1. Introduction

Fluphenazine is a phenothiazine antipsychotic drug with pipearzine derived substituent that is used to treat schizophrenia and bipolar disorder [1]. This drug also has a number of novel and important biological properties [2]. It is worth noting that fluphenazine and melamine generate complexes that have both positive and negative pharmacological side effects [3]. Ding et al. reported a high efficiency phenothiazine for solar cell [4]. Petrus et al. reported XRD structure of fluphenzine dichloride dimethanol solvate [5]. Phenothiazine is a non planar confirmation of the butterfly or bent kind [6]. Drugs of phenothiazine family have a wide range of biological characteristics [7–14]. Promazine has been determined using a variety of methods, including electrophoresis, spectro-photometry and electrochemistry [15–18]. Promazine is used to treat psychiatric disorders and cancer [19–24]. The charge transfer properties, detection by graphene sensors and molecular recognition of phenothiazine derivatives are reported [25–30]. Trifluoperazine, an antipsychotic drug has recently been confirmed

to interact with bovine serum albumin [31]. The production of a nanocomposite for promazine removal from water was reported [32]. Recently, researchers reported sulphide-metal nanocomposites synthesis for the detection of promazine and trifluoperazine [33,34]. The uses of trifluoperazine in medicine have recently been reported [35,36].

Drug research and development rely heavily on quantum chemistry theory, DFT, molecular models and vibrational spectroscopy [37]. Docking studies give the binding and interaction between ligand and receptor, as well as drug mechanism [38]. To understand the action of drugs and proteins, MD simulations can show the oscillations of receptors and ligands [39]. As a result, docking with MD simulation may be utilized to examine the structural properties and binding mechanism of ligands and receptors in a complete and systematic manner. DFT studies of FDD cover new information about their electronic, structural features and reactivity in addition to reactivity analysis and MD simulations. DFT is also used to achieve the highest precision results of FDD's properties in variety of utilizable eco-solvents [40].

---

* Corresponding author.
  E-mail address: jsalotabi@pnu.edu.sa (J.S. Al-Otaibi).
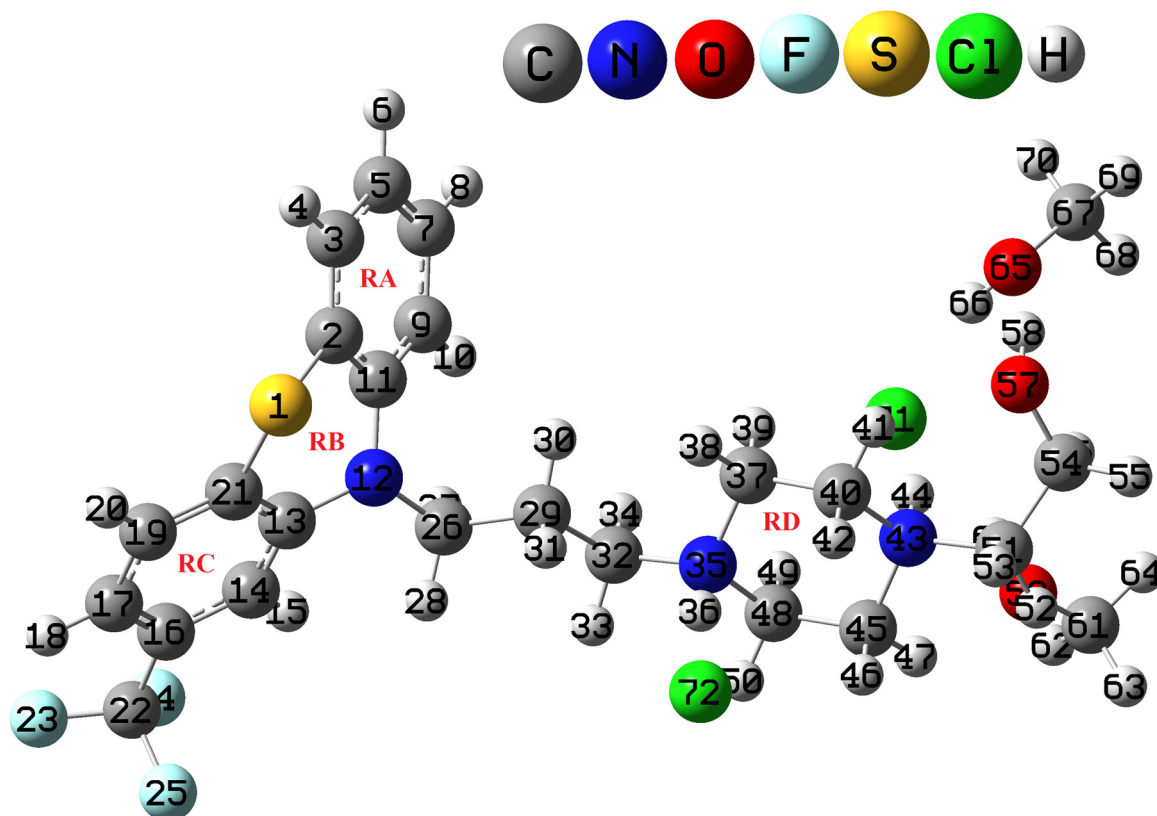
Fig. 1. Optimized molecular structure of FDD.

2. Methods

FDD is obtained as a gift [5] and vibrational spectra (Figs. S1 and S2) were recorded according to literature [41]. Gaussian 09 package was used to perform all quantum chemical calculations with B3LYP/6-311++G* for FDD (Fig. 1) [42–44]. The FMO was used to calculate the DFT-based reactivity descriptors by obtaining ionization energy and electron affinity. NBO analysis was carried out in order to predict the important intra molecular interactions, nature and charge transfers within FDD [45]. Various solvents are being used in the current study to examine the properties of electrons in FDD [46]. HOMO-LUMO and UV analyses are done in different solvents using the IEFPCM model.

Molecular Docking studies are carried out for FDD with SARS-CoV-2 main protease (PDB ID: 6LU7) with highest resolution 1.25 Å [47] and subsequently cleaned for any steric clashes, intrinsic water and co-crystallized molecules. Then the protein structure was subjected to energy minimization using 1000 steps of conjugate gradient algorithm. All the hydrogen are properly added and saved in pdb format for molecular docking purpose. Docking studies were carried out in patch dock web server [48]. Grid centre was provided as 0.35 Å x 6.0 Å x 3.0 Å. Docking parameters were

set for protein small ligand with clustering RMSD 0.5 Å. Ligand binding site information was uploaded in the server advanced parameter option and energy minimized protein and geometrically. The MD simulations studies were carried on the dock complex for FDD with protein (PDB ID: 6LU7) using the Desmond 2020.2 from Schrödinger, LLC as reported earlier [49–55]. The RMSD, Rg, RMSF and SASA) were calculated to monitor the stability of the MD simulations.

3. Results and discussion

3.1. . Spectroscopic and electronic properties

The phenyl ring modes (Table S1) are assigned at: 3075 (IR), 3082 (Raman), 3100, 3093, 3082, 3074 cm^{-1} (DFT) (υCH), 1587, 1448 (IR), 1594, 1590, 1469 (Raman), 1596, 1589, 1470, 1447, 1268, 1049 cm^{-1} (DFT) (υRA); 1041,1241 (IR), 1128, 1040 (Raman), 1244, 1150, 1126, 1039 cm^{-1} (DFT)(δCH) and at 959, 854, 736 (IR), 961, 922, 850, 738 cm^{-1} (DFT) (γCH) for 1,2-substituted ring RA; 3111 (IR), 3112, 3111, 3088 cm^{-1} (DFT) (υCH); 1623, 1605, 1424, (IR), 1627 (Raman), 1622, 1609, 1500, 1422, 1291, 1047 cm^{-1} (DFT) (υRC); 1284 (IR), 1283, 1139, 1047 cm^{-1} (DFT)(δCH) and at 886,

Table 1
Calculated chemical descriptors (eV) of FDD.

Molecular descriptors	Gas	Water	Acetone	DMSO	Methanol	Toluene
E$_{HOMO}$	-5.5140	-5.5140	-5.5119	-5.5132	-5.5127	-5.5285
E$_{LUMO}$	-0.8808	-0.8808	-0.8762	-0.8797	-0.8784	-0.8705
Energy gap	4.6332	4.6332	4.6357	4.6335	4.6343	4.6580
Ionization potential	5.5140	5.5140	5.5119	5.5132	5.5127	5.5285
Electron affinity	0.8808	0.8808	0.8762	0.8797	0.8784	0.8705
Chemical hardness	2.3166	2.3166	2.3179	2.3168	2.3172	2.3290
Chemical potential	-3.1974	-3.1974	-3.1941	-3.1965	-3.1956	-3.1995
Electrophilicity index	2.2065	2.2065	2.2007	2.2050	2.2034	2.1977

Table 2
Theoretical electronic transition parameters of FDD.

solvents	Wavelength (nm)	Band gap (eV)	Energy (cm^{-1})	Oscillator strength (f)	Symmetry	Major contributions
Gas	276.72	4.4805	36137.67	0.065	Singlet-A	HOMO→L+2 (85%)
	322.86	3.8402	30973.30	0.0116	Singlet-A	HOMO→L (92%)
Water	276.72	4.4805	36137.67	0.065	Singlet-A	HOMO→L+2 (85%)
	322.86	3.8402	30973.30	0.0116	Singlet-A	HOMO→L (92%)
DMSO	276.91	4.4774	36112.67	0.070	Singlet-A	HOMO→L+2 (86%)
	322.91	3.8396	30968.46	0.0122	Singlet-A	HOMO→L (92%)
Acetone	277.03	4.4755	36097.34	0.0672	Singlet-A	HOMO→L+2 (86%)
	322.72	3.8419	30987.01	0.0118	Singlet-A	HOMO→L (92%)
Toluene	279.09	4.4425	35831.18	0.0800	Singlet-A	HOMO→L+2 (87%)
	321.37	3.8580	31116.87	0.0133	Singlet-A	HOMO→L (91%)
Methanol	276.85	4.4784	36120.73	0.0651	Singlet-A	HOMO→L+2 (85%)
	322.77	3.8413	30982.18	0.0116	Singlet-A	HOMO→L (92%)

818 (IR), 888 (Raman), 886, 874, 820 (DFT) cm^{-1} (γCH) for 1,2,4-substituted phenyl ring RB [56–58].

The stretching modes of piperazine ring RD are at 1009, 945, 931 (IR), 1006, 947, 931 (Raman) and 1141, 1074, 1062, 1007, 943, 930 cm^{-1} (DFT). The associated CH2 modes are at: 2993 (IR), 2986 (Raman), 3069-2983 cm^{-1} (DFT) (υCH2); 1394, 1356, 1302, 1027, 969, 796, 750 (IR), 1190, 822, 782 (Raman), 1408-750 cm^{-1} (DFT) (δCH2). The bands at 1356 and 1027 cm^{-1} in IR are characteristic modes of bending of CH2. The other CH2 modes of FDD are at: 2868 (IR), 3062, 2980, 2890 (Raman), 3061-2886 cm^{-1} (DFT) (υCH2); 1474, 1335, 1312, 1261, 1241, 1217, 1120, 868 (IR), 1333, 1310, 1278, 1241, 1228, 865 (Raman), 1484-866 cm^{-1} (DFT) (δCH2) [56,59,60].

Other important functional group modes are: υNH...Cl – 2910, 2129 cm^{-1} (DFT), 2219 (IR), 2125 (Raman); δNH...Cl: 1508, 1495, 1490, 1472 cm^{-1} (DFT); υOH – 3487, 3465, 3350 cm^{-1} (DFT), 3433, 3274 (IR), 3404, 3345 (Raman); υCS – 728, 678 cm^{-1} (DFT), 727, 677 (IR), 727, 678 (Raman); υCF at 1163, 1137, 1077 cm^{-1} (DFT), 1164, 1137, 1078 (IR), 1077 cm^{-1} (Raman); δCF at 562, 513, 430, 382, 274 cm^{-1} (DFT); υCO – 1063, 1057, 1033 cm^{-1} (DFT), 1064 (IR), 1055 cm^{-1} (Raman) [56,61,62]. The other deformation modes are also identified.

The solvation energies, changes in enthalpy and Gibbs energy of FDD are, respectively, -5.85, -5.97, -6.76 (acetone), -1.42, -1.45, -1.68 (DMSO) and -2.94, -3.01, -3.44 (methanol) and -53.46, -59.15, -44.31 kJ/mol (toluene) and the values show that the toluene is the best solvent for FDD [63]. The quantum chemical parameters were determined though theoretical calculations using the DFT method (Table 1). Fig. 2 shows that the FDD's HOMO and LUMO are distributed almost throughout the rings except piperazine, indicating a high ability to donate and receive electrons [64,65]. The orbitals of the FDD differ noticeably between the gas and solvent phases. The observed higher hardness value (2.3166) in the gas phase of FDD shows the chemical stability. In the gas state of FDD, energy gap, ionization potential and electron affinity are 4.6332, 5.5140, 0.8808 eV, respectively. When comparing descriptors in solvent state, toluene has high energy gap of 4.6380 eV and a hardness value of 2.3290. The highest and lowest ionization potential values are for toluene (5.5285) and for acetone (5.5119) [66].

UV-Vis spectroscopy is used to investigate the electronic transitions [67] and the electron spectrum of FDD was computed using the IEFPC solvation model in different solvents (Fig. S3) at the B3LYP/6-311++G* level of theory. It is used to calculate FDD's band gap and higher values indicate that tightly bound valence electrons with nucleus [68]. Gas and water get the same wavelength 276.72 nm, band 4.4805 eV, energy 36137.67 cm^{-1} and oscillatory strength 0.065 with contribution 85% (Table 2). Toluene has highest absorption at 279.09 nm, band gap 4.4425 eV and a transition from HOMO to LUMO+2 (87%) giving aromaticity and biological activity of FDD. The conventional hybrid functionals, like B3LYP are

known to underestimate excitation energies in organic systems according to literature [69–71]. The range-separated TDDFT methods give more accurate calculations compared to conventional hybrid DFT methods.

Due to lone pair electrons strong NBO interactions (Table S2) occurred in FDD as: N12→(C9-C11, C13-C21) with energies, 23.23 and 23.25 kcal/mol; O65→(O57-H58) with energy 23.47; Cl71→(N43-H44) with energy 29.98 and other donor (acceptor) orbials of C2-C3 (C9-C11), C5-C7 (C2-C3), C9-C11 (C5-C7), C13-C21 (C17-C19), C14-C16 (C13-C21), C17-C19 (C13-C21), C17-C19 (C14-C16) with energies, 20.85, 22.90, 20.85, 20.51, 21.20, 20.15, 22.40 kcal/mol and 100% p-character in F23, F24, F25, Cl72, O62 atoms of FDD.

3.2. Topological properties of electron density

Bader the pioneer proposed the Atoms in Molecules theory [72] in order to get abundant details about the atoms, molecules, chemical bonding and their topological properties such as electron density (ED) and Laplacian of the electron density (LED). The ED values are given in Table S3. Bond (3, -1), ring (3, +1) and cage critical points (3, +3) present in FDD (Fig. 3) and the range of ED and LED for C−C bonds is 1.549 - 2.024 e/Å^3 and -13.877- -22.001 e/Å^5. The varying charge density values suggest that nature of single and double bonds of the C atoms present in FDD and the charge environments around all the carbon atoms might be different [73].

In FDD, among the C−O bonds, the C54-O57 bond has the slightly high value of charge density (1.631 e/Å^3) when compared to the other bonds. Similarly, among C−N bonds, the C11-N12 and C26-N12 bonds have higher electron density (1.751 e/Å^3, 1.774 e/Å^3) than the remaining C-N bonds. All the C-H bonds have slight variation in their charge density and Laplacian values which suggests that the charge concentrations at the bond path between the atoms might be same. The two C−S bonds are having almost equal charge density value which suggests the similar accumulation of charges in between the atoms. The Cl-H atoms exhibiting closed shell interactions since their Laplacian values are positive. All the three C−F bonds are having similar ED as well as LED. The bonding regions between C and F atoms are visible through the Laplacian, ELF, electron density and LOL maps (Fig. 4(a–d)).

The cylindrical nature of the C−H and C−O bonds has been revealed through their corresponding ellipticity values whereas the π character of the C−C, C−F and C−S bonds are visible through the increased ellipticity values [74].

3.3. Atomic charges and electrostatic potential

The distributions of charges among the atoms present in FDD have been calculated through AIM analysis and listed in the Ta-
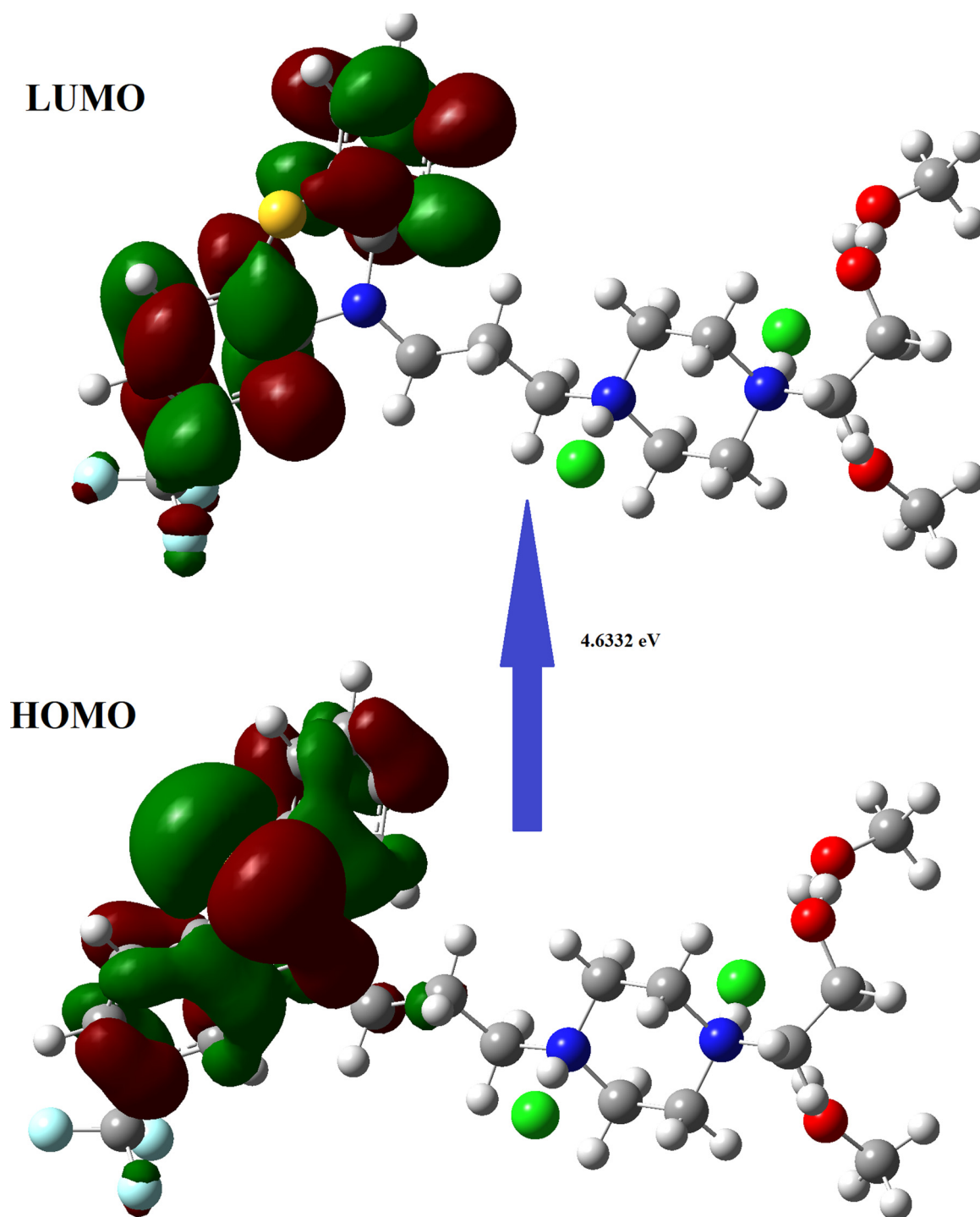
Fig. 2. HOMO-LUMO plots of FDD.

ble S4. In FDD, C22 possesses the highest positive charge of 1.646e since it is attached with F23, F24 and F25 (electronegative atoms). The H44 atom possesses the highest negative charge value of -5.070e which is attached with the N43 atom. Among the Cl atoms, the Cl72 atom has the highest negative charge value (-0.830e) when compared to the Cl71 atom which has the charge value of -0.199e.

The regions of positive and negative electrostatic potentials are helpful to find out the sites of electrophilic as well as nucleophilic attack which is likely happened between the biomolecule and the target protein [75]. A large region of electronegative is seen around

the O atoms and small electronegative cloud is seen around N atoms. The remaining other atoms have been surrounded by large electropositive region. The electrostatic potential map is given in Fig. 5 [76].

3.4. Reduced density gradient

The RDG provides non-covalent and space weak interactions in the molecule [77]. The Multiwfn program [78] has been employed to sketch the RDG and scatter graph and for FDD which is given in
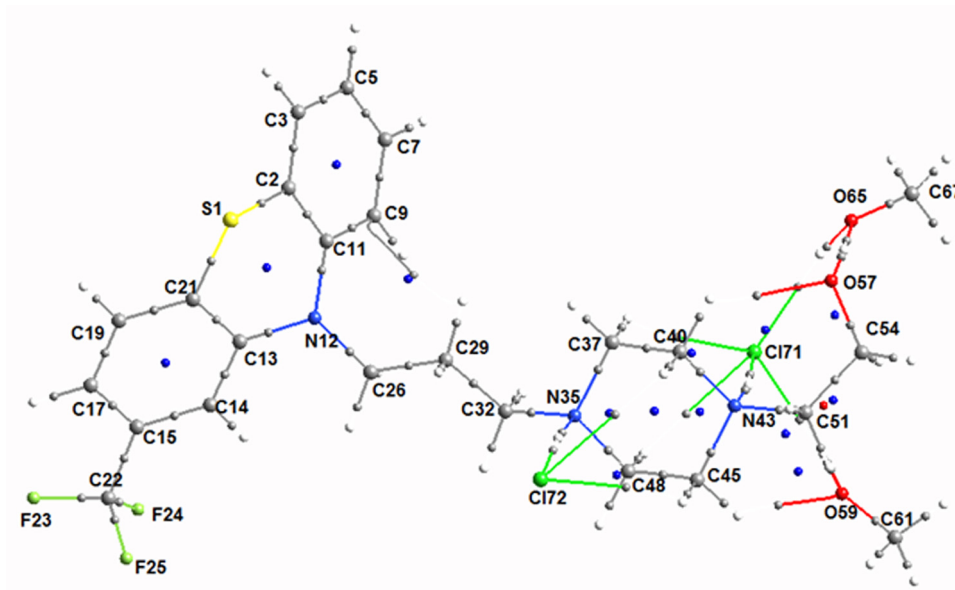
Fig. 3. Molecular graph of the molecule showing critical points.
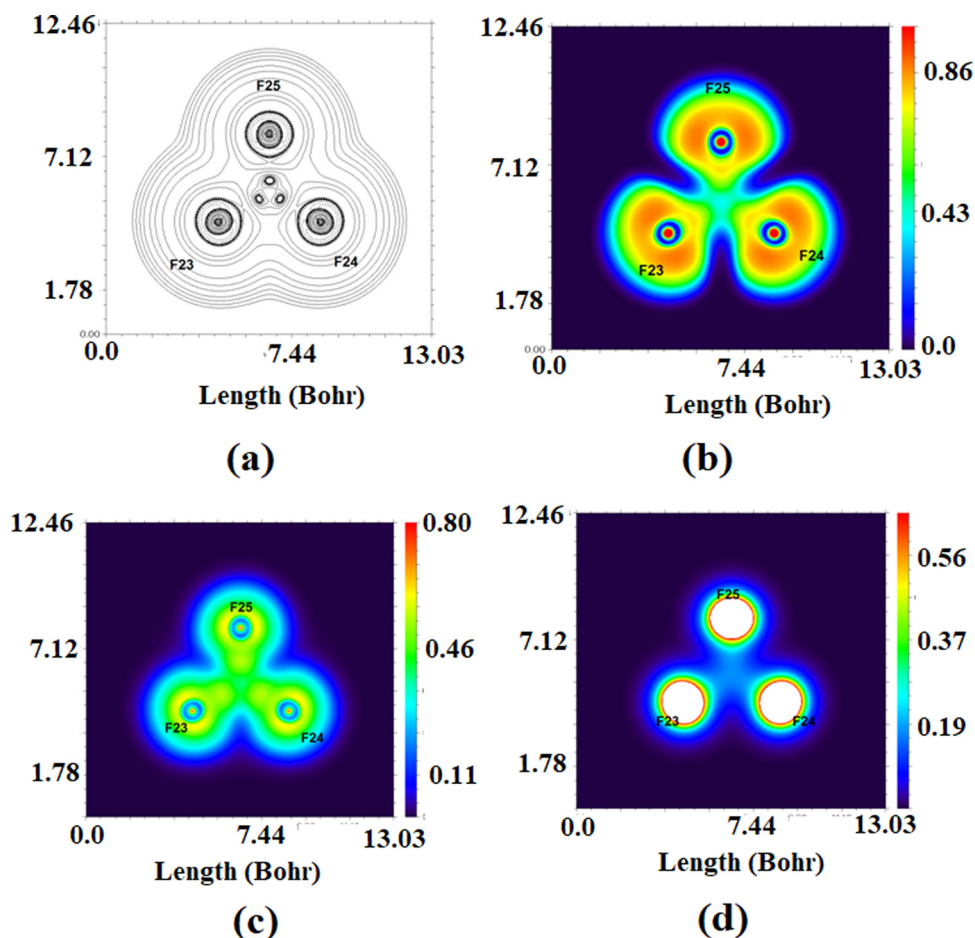
Fig. 4. (a) Laplacian of the electron density (b) view of electron localization function of the plane F23-F24-F25 (c) Electron density (d) LOL of the electron density of the plane F23-F24-F25.

Fig. S4. The 2-dimensional scatter plots of RDG versus $(\lambda_2)\ \rho(r)$ integrated on Fig. S4 shows fingerprints of non-covalent interactions in FDD. On left region of Fig. S4, strong attraction, H bond and halogen bond regions are portrayed, whereas the Van der Waals interactions are visualized in the central part and steric repulsion is visible at right hand side.

3.5. Pharmacology, docking and molecular dynamics simulations

FDD's drug resemblance is investigated to assess its potential for use as a functional ingredient in pharmacological products. Lipinski's rule, also known as the rule of five, has been used to investigate the relationship between the drug similarity of FDD and the
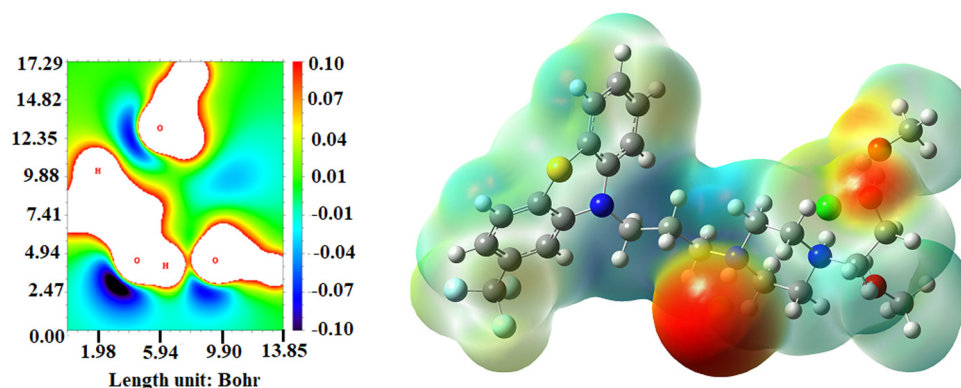
Fig. 5. Electrostatic potential of FDD.
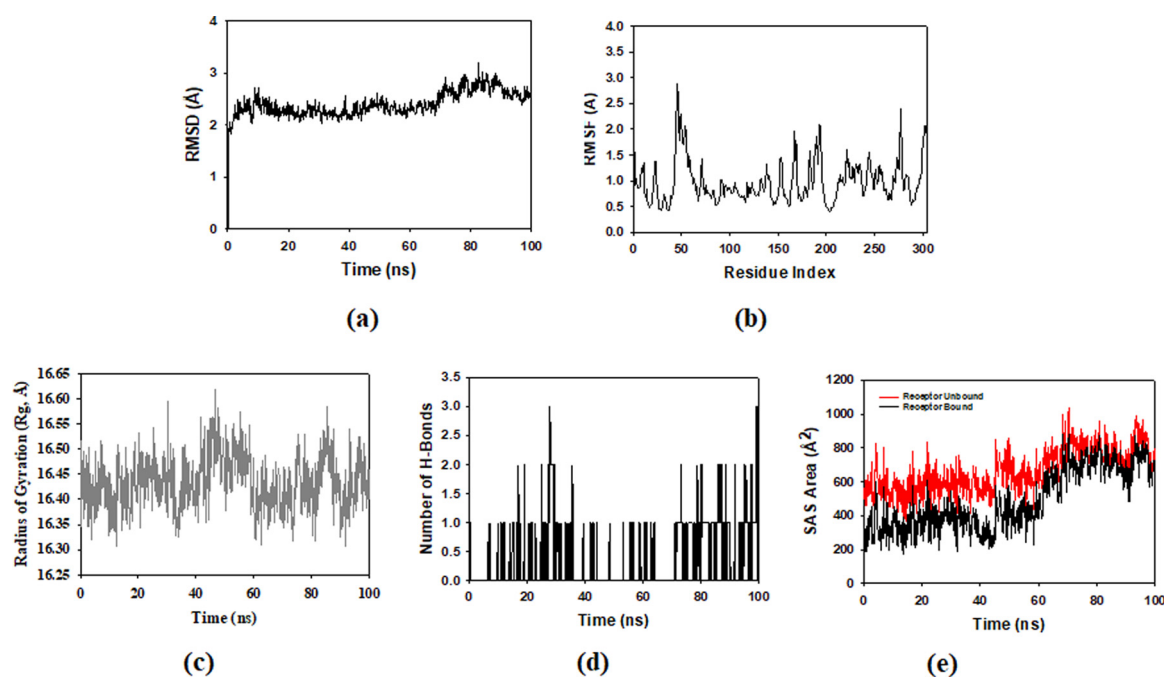
Fig. 6. (a) RMSD plot displaying the molecular vibration of Cα backbone of 6LU7+FDD (b) RMSF plots showing the fluctuations of respective amino acids throughout the simulation time 100 ns for 6LU7+FDD (C) Radius of gyration plots for the deduction of compactness of protein 6LU7+FDD (d) Number of hydrogen bonds formed between 6LU7 and FDD during 100 ns simulation time scale (e) Solvent accessible surface area (SASA) displaying the ligand bound and unbound area at the binding pocket 6LU7+FDD.

oral effects. The FDD is validated according to rule 5 (Table S5). The hydrogen bond donors (5) and acceptors (6), TPSA (113.29Å^2), molecular weight (576.54 g/mol), refractivity (156.09), Lipinski violation (1) and biological score (0.55) are parameters of FDD which are within the threshold values. These parameters of FDD lead to the conclusion that it has a high potential for use as a drug [79,80].

Molecular docking studies of FDD with 6LU7 are displayed in Fig. S5. Surface view of FDD with 6LU7 displayed that FDD well accommodated within in the binding pocket (Fig. S5). The major residues interacted with FDD at the binding pocket of protein Arg222 forming conventional hydrogen bond, halogen bonds with ARG217 and TRP218 and rest are in non bonded vander Waal's interaction. The dock score is calculated within 0.5 Å RMSD clusters tolerence is -8.7 kcalmol^{-1} within the binding pocket area, 586.40.

To determine the stability and convergence of 6LU7+FDD complex, MD simulation studies were performed for 100 ns. When the RMSD values were compared, the simulation of 100 ns revealed stable conformation. A deviation of 0.5 Å is observed for the Cα-backbone of 6LU7 bound to FDD (Fig. 6a). The RMSD plots are in the acceptable range, indicating that 6LU7 is stable in the FDD bound state before and after simulation, and quite stable due to FDD's higher affinity. The RMSF plot gives a significant spike of fluctuation (2.0 Å) at amino acid residue 50 and 275 in 6LU7 while remaining residues show less fluctuation during 100 ns which gives a stable amino acid conformation for the entire period of simulation (Fig. 6b). It means 6LU7 structures are stable during simulation in FDD bound conformations. Radius of gyration of 6LU7 Cα-backbone is lowered from 26.45 Å to 26.40 Å in the 6LU7+FDD complex and this is an indication of the compactness of 6LU7+FDD complex (Fig. 6c). The stable Rg peak thus confirms compactness of 6LU7 in FDD bound state. According to the overall quality analysis based on RMSD and Rg, FDD bound to the 6LU7 target posthumously in the binding cavities and gives stability. The number of H-bonds showed significant numbers between 6LU7 and FDD (Fig. 6d). The complex's stability is aided by a consistent numbers of hydrogen bonds formed between protein and FDD. The accessible solvent surface area gives information about the compactness of FDD-6LU7. The lowering of SASA in case of FDD bound to 6LU7 as compared to unbound state signifies the achievement of stable converged structures due to high compactness of both the systems (Fig. 6e) [81–84].

4. Conclusion

We used theoretical and experimental methods to investigate the spectroscopic properties of FDD in this study. The FDD drug contains reactive sites are identified on O and N atoms. The UV-Vis spectrum shows maximum absorption wavelengths with solvent toluene, which is superior to other solvents. In FDD, C54-O57 bond has the slightly high value of charge density when compared to the other bonds and among the C-N bonds, the C11-N12 and C26-N12 bonds have higher electron density. The ADMET and drug-likeness properties of FDD demonstrate its intoxicating nature.Molecular docking studies confirm the protein-FDD H bond interaction with binding energy of -8.70 kcal/mol. The lowering of SASA for FDD-6LU7 as compared to unbound state gives a stable converged structure. Hence the FDD compound can be a potential drug candidate for SARS-CoV-2 main protease.

Declaration of Competing Interest

The authors declare no conflict of interest.

CRediT authorship contribution statement

Jamelah S. Al-Otaibi: Conceptualization, Methodology, Data curation, Writing – original draft, Software, Validation. **Y. Sheena Mary:** Conceptualization, Methodology, Data curation, Writing – original draft, Software, Validation. **Y. Shyma Mary:** Conceptualization, Methodology, Data curation, Writing – original draft, Software, Validation. **R. Niranjana Devi:** Conceptualization, Methodology, Data curation, Writing – original draft, Software, Validation. **Sreejit Soman:** Conceptualization, Methodology, Data curation, Writing – original draft, Software, Validation.

Data availability

Data will be made available on request.

Acknowledgments

Supplementary materials

Supplementary material associated with this article can be found, in the online version, at doi:10.1016/j.molstruc.2022.133633.

References

[1] M. Otreba, A. Beberok, D. Wrzesniok, E. Buszman, *In vitro* melanogenesis inhibition by fluphenazine and prochlorperazine in normal human melanocytes lightly pigmented, DARU J. Pharm. Sci. 26 (2018) 85–89, doi:10.1007/s40199-018-0206-4.

[2] C.H. Wu, L.Y. Bai, M.H. Tsai, P.C. Chu, C.F. Chiu, M.Y. Chen, S.J. Chiu, J.H. Chiang, J.R. Weng, Pharmacological exploitation of the phenothiazine antipsychotics to develop novel antitumor agents-A drug repurposing strategy, Sci. Rep. 6 (2016) 27540, doi:10.1038/srep27540.

[3] H. Ando, Y. Niki, M. Ito, K. Akiyama, M.S. Matsui, D.B. Yaroh, M. Ichihashi, Melanosomes are transferred from melanocytes to keratinocytes through the processes of packing, release, uptake and dispersion, J. Invest. Dermatol. 132 (2012) 1222–1229, doi:10.1038/jid.2011.413.

[4] X. Ding, H. Wang, C. Chen, H. Li, Y. Tian, Q. Li, C. Wu, L. Ding, M.Cheng X.Yang, Passivation functionalized phenothiazine-based hole transport material for highly efficient perovskite solar cell with efficiency exceeding 22%, Chem. Eng. J. 410 (2021) 128328, doi:10.1016/j.cej.2020.128328.

[5] J. Petrus, R. Petrus, B. Czarnik-Matusewicz, Fluphenzine dichloride dimethanol solvate, Acta Cryst. E68 (2012) o1004–o1005, doi:10.1107/S1600536812008707.

[6] P.S. Gangadhar, G. Reddy, S. Prasanthkumar, L. Giribabu, Phenothiazine functional materials for organic optoelectronic applications, Phys. Chem. Chem. Phys. 23 (2021) 14969, doi:10.1039/d1cp01185e.

[7] B.M. Mlodawska, K. Suwinska, K. Pluta, M. Jelen, 10-(3′-Nitro-4′-pyridyl)-1,8-diazaphenothiazine as the double Smiles rearrangement product, J. Mol. Struct. 1015 (2012) 94–98, doi:10.1016/j.molstruc.2012.02.022.

[8] Y. Mizuno, K. Sato, T. Sano, R. Kurihana, T. Kojima, Y. Yamakawa, A. Ishii, Y. Katsumata, Identification and characterization of 17 phenothiazine compounds by capillary high performance liquid chromatography/fast atom bombardment mass spectrometry, Leg. Med. 4 (2002) 207–216, doi:10.1016/S1344-6223(02)00051-2.

[9] I.M. Tsakovska, QSAR and 3D-QSAR of phenothiazine type multidrug resistance modulators P388/ADR cells, Bioorg. Med. Chem. 11 (2003) 2889–2899, doi:10.1016/S0968-0896(03)00222-0.

[10] A. Zineb, B. Salah, M. Nadjib, B. Salima, B. Lofti, Structure activity relationship and quantitative structure activity relationships modeling of cyto-toxicity of phenothiazine derivativees, Quantum Matter 5 (2016) 124–129, doi:10.1166/qm.2016.1264.

[11] T. Takada, K. Kawai, M. Fujitsuka, T. Majima, Rapid long distance hole transfer through consecutive adenine sequence, J. Am. Chem. Soc. 128 (2006) 11012–11013, doi:10.1021/ja0641554.

[12] E.A. Weiss, M.J. Ahrens, L.E. Sinks, M.A. Ratner, M.R. Wasielewski, Solvent control of spin dependent charge recombination mechanisms within donor conjugated bridge acceptor molecules, J. Am. Chem. Soc. 126 (2004) 9510–9511, doi:10.1021/ja047205i.

[13] G.W. Kim, M.J. Cho, Y.J. Yu, Z.H. Kim, J.I. Jin, D.Y. Kim, D.H. Choi, Red emitting phenothiazine dendrimers encapsulated 2-{2-[2-(4-dimethylaminophenyl)vinyl]-6-methylpyran-4-ylidene}malononitrile derivatives, Chem. Mater. 19 (2007) 42–50, doi:10.1021/cm0618493.

[14] S. Imabayashi, K. Ban, T. Ueki, M. Watanabe, Comparison of catalytic electrochemistry of glucose oxidase between covalently modified and freely diffusing phenothiazine labeled poly(ethylene oxide) mediator systems, J. Phys. Chem. B 107 (2003) 8834–8839, doi:10.1021/jp034189n.

[15] D.C. Le, C.J. Morin, M. Beljean, A.M. Siouffia, P.L. Desbene, Electrophoretic separations of twelve phenothiazines and N-dimethyl derivatives by using capillary zone electrophoresis and micellar electrokientic chromatography with nonionic surfactant, J. Chromatogr. A 1063 (2005) 235–240, doi:10.1016/j.chroma.2004.11.056.

[16] J. Karpinska, H.P. Tarasiewicz, Application of the coupled redox and complexation reactions to flow injection spectrophotometric determination of promazine, Anal. Lett. 30 (1997) 2365–2375, doi:10.1080/00032719708001748.

[17] B. Zeng, F. Huang, Electrochemical behaviour and determination of fluphenazine at multi walled carbon nanotubes/(3-mercaptopropyl) trimethoxysilane bilayer modified gold electrodes, Talanta 64 (2004) 380–386, doi:10.1016/j.talanta.2004.02.024.

[18] M. Jabli, N. Tka, K. Ramzi, T.A. Saleh, Physicochemical characteristics and dyeing properties of lignin-cellulose fibers derivd from Nerium oleander, J. Mol. Liq. 249 (2018) 1138-1114, doi:10.1016/j.molliq.2017.11.126.

[19] J.A. Cogordan, M. Mayoral, E. Angeles, R.A. Toscano, R. Martinez, Neuroleptic and antidepressant tricyclic compounds: Theoretical study for predicting their biological activity by semiempirical density functional, and Hartree-Fock methods, Int. J. Quantum Chem. 71 (1999) 415–432, doi:10.1002/(SICI)1097-461X(1999)71:5⟨415::AID-QUA3⟩3.0.CO;2-0.

[20] D. Pan, L.C.T. Shoute, D.L. Phillips, Time resolved resonance Raman and density functional study of the radical cation of promazine, J. Phys. Chem. A 103 (1999) 6851–6861, doi:10.1021/jp991342y.

[21] M. Wainwright, H. Mohr, W.H. Walker, Phenothiazinium derivatives for pathogen inactivation in blood products, J. Photochem. Photobiol. B 86 (2007) 45–58, doi:10.1016/j.jphotobiol.2006.07.005.

[22] B.M. Mlodawska, K. Pluta, M. Jelen, Estimation of the lipohilicity of new anticancer and immunosuppresive 1,8-diazaphenothiazine derivatives, J. Chromatogr. Sci. 53 (2015) 462–466, doi:10.1093/chromsci/bmu065.

[23] K. Pluta, M. Jelen, B.M. Mlodawska, M. Zimecki, J. Artym, M. Kocieba, Anticancer activity of newly synthesized azaphenothiazines from NCI's anticancer screnning bank, Pharmacol. Rep. 62 (2010) 319–332, doi:10.1016/S1734-1140(10)70272-3.

[24] B.M. Mlodawska, K. Pluta, M. Latocha, M. Jelen, D. Kusmierz, Synthesis and anticancer and lipophilic properties of 10-dialkylaminobutynyl derivatives of 1,8- and 2,7-diazaphenothiazines, J. Enzyme Inhib. Med. Chem. 31 (2016) 1132–1138, doi:10.3109/14756366.2015.1101092.

[25] A. Kinal, N. Acar, A DFT and TD-DFT study on intermolecular charge transfer complexes of pyrene with phenothiazine and promazine, J. Mol. Struct. THEOCHEM 949 (2010) 36–40, doi:10.1016/j.theochem.2010.02.033.

[26] K.A. AlAqad, R. Suleiman, O.C.S. Al Hamouz, T.A. Saleh, Novel graphene modified carbon-paste electrode for promazine detection by sqaure wave voltametry, J. Mol. Liq. 252 (2018) 75–82, doi:10.1016/j.molliq.2017.12.108.

[27] J. Haginaka, K. Nishimura, T. Kimachi, K. Inamoto, Y. Takemoto, Y. Kobayaashi, Retention and molecular recognition mechanisms of molecularly imprinted polymers for promzine derivatives, Talanta 205 (2019) 120149, doi:10.1016/j.talanta.2019.120149.

[28] T.S. Raman, N. Acar, Interactions of promazine with selected biomolecules: photophysical and computational investigation, Chem. Phys. 517 (2019) 161–176, doi:10.1016/j.chemphys.2018.10.010.

[29] M.E.M. Hassouna, A.M. Adawi, E.A. Ali, Extractive spectrophotometric determination of chlorpromazine and trifluoperazine hydrochloride in pharmaceutical preparations, Egypt. J. Forensic Sci. 2 (2012) 62–68, doi:10.1016/j.ejfs.2012.04.001.

[30] K.G. Krishnan, C.U. Kumar, W.M. Lim, C.W. Mai, P.V. Thanikachalam, C. Ramalingan, Novel cyanoacetamide integrated phenothiazines: synthesis, char-

acterization, computational studies and *in vitro* antioxidant and anticancer evaluations, J. Mol. Struct. 1199 (2020) 127037, doi:10.1016/j.molstruc.2019.127037.

[31] D. Raghav, S. Mahanty, K. Rathinasamy, Characterizing the interactions of the antipsychotic drug trifluoperaizne with bovine serum albumin: Probing the drug-protein and drug-drug interactions using multi-spectroscopic approaches, Spectrochim. Acta 226 (2020) 117584, doi:10.1016/j.saa.2019.117584.

[32] B. D'Cruz, M. Madkour, M.O. Amin, E. Al-Hetlani, Efficient and recoverable magnetic AC-Fe$_3$O$_3$ nanocomposite for rapid removal of promazine from waste water, Mater. Chem. Phys. 240 (2020) 122109, doi:10.1016/j.matchemphys.2019.122109.

[33] R. Sakthivel, M. Annalakshmi, S.M. Chen, S. Kubendhiran, Synergistic activity of binary metal sulphide WS2-RuS2 nanospheres for the electrochemical detection of the antipsychotic drug promazine, New J. Chem. 44 (2020) 4621–4630, doi:10.1039/D0NJ00096E.

[34] A. Sangili, R. Sakthivel, S.M. Chen, Cost effective single step synthesis of flower like cerium-ruthenium-sulfide for the determination of antipsychotic drug trifluoperazine in human urine samples, Anal. Chim. Acta 1131 (2020) 35–44, doi:10.1016/j.aca.2020.07.032.

[35] X. Zhang, K. Ding, J. Ji, H. Parajuli, SN. Aasen, H. Espedal, B. Huang, A. Chen, J. Wang, X. Li, F. Thorsen, Trifluoperazine prolongs the survival of experimental brain metastases by STAT3-dependent lysosomal membrane permeabilization, Am. J. Cancer Res. 10 (2020) 545–563 PMID: 32195026.

[36] A. Kiani, S.H. Nik, A. Khodadoost, A. Salimi, J. Pourahmad, Trifluoperazine an antipsychotic drug and inhibitor of mitochondrial permeability transition protects cytarabine and ifosfamide-induced neurotoxicity, Drug Res. 70 (2020) 265–272, doi:10.1055/a-1154-8672.

[37] L.G. Ferreira, R.N.D. Santos, G. Oliva, A.D. Andricopulo, Molecular docking and structure based drug design strategies, Molecules 24 (2015) 13384–13421, doi:10.3390/molecules200713384.

[38] Y. Cai, N.K. Yilmaz, W. Myint, R. Ishima, C.A. Schiffer, Differential flap dynamics in wild-type and a drug resistant variant of HIV-1 protease revealed by molecular dynamics and NMR relaxation, J. Chem. Theory Comput. 8 (2012) 3452–3462, doi:10.1021/ct300076y.

[39] M.D. Tiezza, F.M. Bickelhaupt, L. Flohe, L. Orian, Proton transfer and SN2 reactions as steps of fast selenol and thiol oxidation in proteins: a model molecular study based on GPx, ChemPlusChem 86 (2021) 524, doi:10.1002/cplu.202000781.

[40] W. Xie, T. Li, C. Chen, H. Wu, S. Liang, H. Chang, B. Liu, E. Drioli, Q. Wang, J.C. Crittenden, Using the green solvent dimethyl sulfoxide to replace traditional solvents partly and fabricating PVC/PVC-g-PEGMA blended ultrafiltration membranes with high permeability and rejection, Ind. Eng. Chem. Res. 58 (2019) 6413–6423, doi:10.1021/acs.iecr.9b00370.

[41] P.S. Binil, Y.S. Mary, H.T. Varghese, C.Y. Panicker, M.R. Anoop, T.K. Manojkumar, Infrared and Raman spectroscopic analyses and theoretical computation of 4-butyl-1-(4-hydroxyphenyl)-2-phenyl-3,5-pyrazolidinedione, Spectrochim. Acta 94 (2012) 101–109, doi:10.1016/j.saa.2012.03.014.

[42] M.J. Frisch, et al. *Gaussian 09, Revision B.01*, Gaussian, Inc., Wallingford CT, 2010.

[43] R. Dennington, T. Keith, J. Millam, Gaussview, Version 5, Semichem Inc., Shawnee Mission, KS, 2009.

[44] A.D. Becke, Density functional thermochemistry. III. The role of exact exchange, J. Chem. Phys. 98 (1993) 5648–5651, doi:10.1063/1.464913.

[45] A.E. Reed, L.A. Curtiss, F. Weinhold, Intermolecular interactions from a natural bond orbital, donor-acceptor viewpoint, Chem. Rev. 88 (1988) 899–926, doi:10.1021/cr00088a005.

[46] A. Thamarai, R. Vadamalar, M. Raja, S. Muthu, B. Narayana, P. Ramesh, R.R. Muhamed, S. Sevvanthi, S. Aayisha, Molecular structure interpretation, spectroscopic (FT-IR, FT-Raman), electronic salvation (UV-Vis, HOMO-LUMO and NLO) properties and biological evaluation of (2E)-3-(biphenyl-4-yl)-1-(4-bromophenyl)prop-2-en-1-one: experimental and computational modelling approach, Spectrochim. Acta 226 (2020) 117609, doi:10.1016/j.saa.2019.117609.

[47] https://www.rcsb.org/structure/6lu7

[48] https://bioinfo3d.cs.tau.ac.il/PatchDock/php.php

[49] K.J. Bowers, D.E. Chow, H. Xu, R.O. Dror, M.P. Eastwood, B.A. Gregersen, J.L. Klepies, I. Kolossvary, M.A. Moraes, F.D. Sacerdoti, J.K. Salmon, Scalable algorithms for molecular dynamics simulations on commodity clusters, in: InSC'06: Proceedings of the 2006 ACM/IEEE Conference on Supercomputing, 2006.

[50] E. Chow, C.A. Rendleman, K.J. Bowers, R.O. Dror, D.H. Hughes, J. Gullingsrud, F.D. Sacerdoti, D.E. Shaw, Desmond performance on a cluster of multicore processors, DE Shaw Research technical report DESRES/TR—2008-01.2008.

[51] D. Shivakumar, J. Williams, Y. Wu, J.Shelley W.Damm, W. Sherman, Prediction of absolute solvation free energies using molecular dynamics free energy perturbation and the OPLS force field, J. Chem. Theory Comput. 6 (2010) 1509–1519, doi:10.1519/ct900587b.

[52] WL. Jorgensen, J. Chandrasekhar, JD. Madura, RW. Impey, M.L. Klein, Comparison of simple potential functions for simulating liquid water, J. Chem. Phys. 79 (1983) 926–935, doi:10.1063/1.445869.

[53] G.J. Martyna, D.J. Tobias, M.L. Klein, Constant pressure molecular dynamics algorithms, J. Chem. Phys. 101 (1994) 4177–4189, doi:10.1063/1.467468.

[54] G.J. Martyna, M.L. Klein, M. Tuckerman, Nose-hoover chains- the canonical ensemble via continuous dynamics, J. Chem. Phys. 97 (1992) 2635–2643, doi:10.1063/1.463940.

[55] Toukmaji, Y. Abdulnour, J. Board, Ewald summation techniques in perspective: a survey, Comput. Phys. Commun. 95 (1996) 73–92, doi:10.1016/0010-4655(96)00016-1.

[56] N.P.G. Roeges, A Guide to the complete Interpretation of Infrared Spectra of Organic Structures, John Wiley and Sons Inc., New York, NY, 1994.

[57] P.R.K. Rani, Y.S. Mary, A. Fernandez, A. Priya, Y.S. Mary, R. Thomas, Single crystal XRD, DFT investigations and molecular docking study of 2-((1,5-dimethyl-3-oxo-2-phenyl-2,3-dihydro-1H-pyrazol-4-yl)naphthalene-1,4-dione as a potential anti-cancer lead molecule, Comput. Biol. Chem. 78 (2019) 153–164, doi:10.1016/j.compbiolchem.2018.11.022.

[58] S.P. Yeddu, T. Pooventhiran, A. Veeraiah, D. Vijay, K.E. Srikanth, A. Irfan, R. Thomas, Vibrational spectral studies, quantum mechanical properties, and biological activity prediction and inclusion molecular self-assembly formation of N-N'-dimethylethylene urea, Biointerface Res. Appl. Chem. 12 (2022) 3996–4017, doi:10.33263/BRIAC123.39964017.

[59] R. Renjith, Y.S. Mary, C.Y. Panicker, H.T. Varghes, M. Pakosinska-Parys, C. Van Alsenoy, A.A. Al-Saadi, Spectroscopic (FT-IR, FT-Raman) investigations and quantum chemical calculations of 1,7,8,9-tetrachloro-10,10-dimethoxy-4-{3-[4-(3-methoxyphenyl)piperazin-1-yl]propyl}-4-azatricyclo[5.2.1.0^{2,6}]dec-8-ene-3,5-dione, Spectrochim. Acta 129 (2014) 438–450, doi:10.1016/j.saa.2014.03.077.

[60] R. Renjith, Y.S. Mary, C.Y. Panicker, H.T. Varghes, M. Pakosinska-Parys, C. Van Alsenoy, T.K. Manojkumar, Spectroscopic (FT-IR, FT-Raman), first order hyperpolarizability, NBO analysis, HOMO and LUMO analysis of 1,7,8,9-tetrachloro-10,10-dimethoxy-4-[3-[4-phenylpiperazin-1-yl]propyl]-4-azatricyclo[5.2.1.0^{2,6}]dec-8-ene-3,5-dione by density functional methods, Spectrochim. Acta 124 (2014) 500–513, doi:10.1016/j.saa.2014.01.045.

[61] N.Z. Alzoman, Y.S. Mary, C.Y. Panicker, I.A. Al-Swaidan, A.A. El-Emam, O.A. Al-Deeb, A.A. Al-Saadi, C. Van Alsenoy, J.A. War, Spectroscopic investigation (FT-IR and FT-Raman), vibrational assignments, HOMO-LUMO, NBO, MEP analysis and molecular docking study of 2-[(4-chlorobenzyl)sulfanyl]-4-(2-methylpropyl)-6-(phenylsuflanyl)-pyrimidine-5-carbonitrile, a potential chemotherapeutic agent, Spectrochim. Acta 139 (2015) 413–424, doi:10.1106/j.saa.2014.12.043.

[62] G. Socrates, Infrared Characteristic Group Frequencies, John Wiley and Sons, New York, 1980.

[63] J.S. Al-Otaibi, Y.S. Mary, Y.S. Mary, S. Soman, N. Acharjee, B. Narayana, Theoreticl and experimental investigation of a pyrazole derivative-solvation effects, reactivity analysis and MD simulations, Chem. Phys. Lett. 793 (2022) 139469, doi:10.1016/j.cplett.2022.139469.

[64] J.S. Al-Otaibi, Y.S. Mary, S. Armakovic, R. Thomas, Hybrid and bioactive cocrystals of pyrazinamide with hydroxybenzoic acids: detailed study of structure, spectroscopic characteristics, other potential applications and noncovalent interactions using SAPT, J. Mol. Struct. 1202 (2020) 127316, doi:10.1016/j.molstruc.2019.127316.

[65] B. Sureshkumar, Y.S. Mary, K.S. Resmi, C.Y. Panicker, S. Armakovic, S.J. Armakovic, C. Van Alsenoy, B. Narayana, S. Suma, Spectroscopic analysis of 8-hydroxyquinoline derivatives and investigation of its reactive properties by DFT and molecular dynamics simulations, J. Mol. Struct. 1156 (2018) 336–347, doi:10.1016/j.molstruc.2017.11.120.

[66] T. Pooventhiran, B.S. Gangadharappa, O.A. Abu Ali, R. Thomas, D.I. Saleh, Study of the structural features and solvent effects using ab initio molecular dynamics and energy decomposition analysis of ATOGEPANT in water and ammonia, J. Mol. Liq. (2022) 118672, doi:10.1016/j.molliq.2022.118672.

[67] B. Badhani, R. Kakkar, DFT study of structural and electronic properties of Gallic acid and its anions in gas phase and in aqueous solution, Struct. Chem. 28 (2017) 1789–1802, doi:10.1007/s11224-017-0958-3.

[68] S.S. Mati, S. Chall, S. Rakshit, S.C. Bhattacharya, Spectroscopic and quantum mechanical approach of solvatochromic immobilization: modulation of electronic structure and excited-state properties of 1,8-naphthalimide derivative, J. Fluorescence 25 (2015) 341–353, doi:10.1007/s10895-015-1516-2.

[69] B.M. Wong, T.H. Hsieh, Optoelectronic and excitonic properties of oligoacenes: substantial improvements from range-separated time-dependent density functional theory, J. Chem. Theory Comput. 6 (2010) 3704–3712, doi:10.1021/ct100529s.

[70] A.E. Raeber, B.M. Wong, The importance of short- and long-range exchange on various excited state properties of DNA monomers, stacked complexes, and Watson-Crick pairs, J. Chem. Theory Comput. 11 (2015) 2199–2209, doi:10.1021/acs.jctc.5b00105.

[71] S.A. Tawfik, X.Y. Cui, S.P. Ringer, C. Stampfl, A TDDFT study of the optical excitation of nucleic acid bases-C complexes, J. Phys. Chem. A 121 (2017) 9058–9063, doi:10.1021/acs.jpca.7b07442.

[72] R.F.W. Bader, Atoms in Molecules: A Quantum Theory, Clarendon Press, Oxford, 1990.

[73] J.S. Al-Otaibi, Y.S. Mary, Y.S. Mary, N. Acharjee, Quantum mechanical investigation into the adsorption pattern of clomipramine and methotrimeprazine HCl with graphene and fullerene, Polycycl. Aromat. Compd. (2022), doi:10.1080/10406638.2022.2041678.

[74] V.S. Kumar, Y.S. Mary, Y.S. Mary, G. Serdaroglu, A.S. Rad, M.S. Roxy, P.S. Majula, B.K. Sarojini, Conformational analysis and DFT investigations of two triazole derivatives and its halogenated substitution by using spectroscopy, AIM and molecular docking, Chem. Data Collect. 31 (2021) 100625, doi:10.1016/j.cdc.2020.100625.

[75] P. Politzer, P.R. Laurence, K. Jayasuriya, Molecular electrostatic potentials: an effective tool for the elucidation of biochemical phenomena, Environ. Health Perspect. 61 (1985) 191–202, doi:10.1289/ehp.8561191.

[76] P. Politzer, J.S. Murray, Computational prediction of condensed phase properties from statistical characterization of molecular surface electrostatic potentials, Fluid Phase Equilib. 185 (2001) 129–137, doi:10.1016/s0378-3812(01)00463-0.

[77] R.A. Boto, J. Contreras-Garcia, J. Tierny, P. Jean-Philip, Interpretation of the reduced density gradient, Mol. Phys. 114 (2016) 1406–1414, doi:10.1080/00268976.2015.1123777.

[78] T. Lu, F. Chen, Multiwfn: a multifunctional wavefunction analyzer, J. Comp. Chem. 33 (2012) 580–592, doi:10.1002/jcc.22885.

[79] C.A. Lipinski, F. Lomlardo, B.W. Dominy, P.J. Feeney, Experimental and computational approaches to estimate solubility and permeability in drug discovery and development settings, Adv. Drug Deliv. Rev. 46 (2001) 3–26, doi:10.1016/s0169-409x(00)00129-0.

[80] C.A. Lipinski, Lead- and drug-like compounds: the rule-of-five revolution, Drug Discov. Today Technol. 1 (2004) 337–341, doi:10.1016/j.ddtec.2004.11.007.

[81] J.S. Al-Otaibi, Y.S. Mary, Y.S. Mary, S. Aayisha, DFT conformational, wavefunction based reactivity analysis, docking and MD simulations of a carboxamide derivative with potential anticancer activity, Polycycl. Aromat. Compd. (2022), doi:10.1080/10406638.2022.2032765.

[82] J.S. Al-Otaibi, R.A. Costa, E.V. Costa, V.L. Tananta, Y. Sheena Mary, Y. shyma Mary, Insights into solvation, chemical reactivity, structural, vibrational and anti-hypertensive properties of a thiazolopyrimidine derivative by DFT and MD simulations, Struct. Chem. 33 (2022) 1271–1283, doi:10.1007/s11224-022-01931-1.

[83] Y.S. Mary, Y.S. Mary, S. Armakovic, S.J. Armakovic, R. Yadav, I. Celik, R. Razavi, Investigation of reactive properties, adsorption on fullerene, DFT, molecular dynamics simulation of an anthracene derivative targeting dihydrofolate reductase and human dUTPase, J. Biomol. Struct. Dyn. (2021), doi:10.1080/07391102.2021.1953602.

[84] J.S. Al-Otaibi, Y.S. Mary, Y.S. Mary, R. Yadav, Structural and reactivity studies of pravadoline – An ionic liquid, with reference to its wavefunction-relative properties using DFT and MD simulations, J. Mol. Struct. 1245 (2021) 131074, doi:10.1016/j.molstruc.2021.131074.